DRAFT: Accretion Product Formation in the Self- and Cross-Reactions of Small Alkene-Derived Hydroxy Peroxy Radicals

Sara E. Murphy, John D. Crounse, Jing Chen, Henrik G. Kjaergaard, and Paul O. Wennberg

Abstract

The formation of a peroxide accretion product (ROOR) in the self- and cross-reactions of peroxy radicals (RO_2) has recently been found to play a more significant role than previously anticipated in a variety of oxidation systems. In this work, we examine the formation of this accretion product in the self- and cross-reactions of RO_2 derived from the OH-initiated oxidation of propene, cis-2-butene, and methylpropene in the presence of ethene. Using CF_3O^- GC-HRToF-CIMS, we measure the formation rate of the various accretion products in each system relative to the formation rate of the ethene-derived ROOR, which was measured in our previous work. We find that the accretion product forms in all of these self- and cross-reactions, and that the ROOR formation rate decreases with increasing substitution and that ROOR formation appears to decrease with increasing carbon chain length. Finally, we compare the reaction rates and ROOR formation rates in self- and cross-reactions and determine that the arithmetic mean of the self-reactions is likely a good method for estimating the ROOR formation in cross-reactions.

Introduction

The oxidation of anthropogenic and biogenic hydrocarbons is one of the primary drivers of tropospheric chemical processes. Upon emission to the atmosphere, these hydrocarbons are primarily oxidized by OH, O_3, or NO_3, followed by addition of O_2 to form peroxy radicals (RO_2).[1] The radical cycling and ultimate fate of these RO_2 has significant implications for, among other important processes, the formation of ozone and particulate matter.[2–4] In polluted areas such as urban centers, where nitrogen oxides (NO_x = NO + NO_2) tend to be high, RO_2 primarily react with NO.[5,6] This reaction leads either to a radical recycling channel, in which NO_2 and an alkoxy radical (RO) are formed, or to the formation of an organic nitrate ($RONO_2$).[7,8] The former propagates the radical cycle that leads to ozone formation, while the latter can lead to the formation of secondary organic aerosol (SOA) or transport of NO_x to regions removed from the original source.[9]

In regions where NO_x is low, RO_2 will undergo unimolecular reaction[10] or bimolecular reactions with (primarily) HO_2 or other RO_2.[7,11] This chemistry is important in remote regions and is even becoming important in urban areas as NO_x continues to decrease due to emission regulations.[12,13] The reaction of RO_2 with HO_2 can, similarly to the reaction with NO, lead to radical propagation (Reaction 1b and 1c) or radical termination (Reaction 1a) via the formation of a hydroperoxide (ROOH).[7]

$$\mathrm{RO_2 + HO_2 \rightarrow ROOH + O_2} \tag{1a}$$

$$\rightarrow \mathrm{RO + OH + O_2} \tag{1b}$$

$$\rightarrow \mathrm{R_{-H}{=}O + HO_2 + OH} \tag{1c}$$

While Reaction 1a is the dominant pathway for most alkyl peroxy radicals, Reactions 1c and 1b have been observed to play an important role in the reactions of oxygenated peroxy radicals, including β-hydroxy peroxy radicals, with HO_2.[11] Although the reaction rates of peroxy radicals with HO_2 and the branching to products remains uncertain for many peroxy

radicals, structure activity relationships suggest that the rate coefficient of the RO_2 + HO_2 reaction largely depends on the number of heavy atoms in the peroxy radical and exhibits little dependence on substitution or structure.[14]

The reaction of RO_2 with R'O_2 (the so-called 'permutation' or cross-reaction, Reaction 2) or with itself (the self-reaction, R = R') proceeds primarily via three reaction pathways: the formation of two alkoxy radicals (Reaction 2a), the formation of an alcohol and a carbonyl (Reaction 2c and 2b), or the formation of a peroxide accretion product (Reaction 2d).[7,11]

$$\mathrm{RO_2 + R'O_2 \rightarrow RO + R'O + O_2} \quad (2a)$$

$$\rightarrow \mathrm{R'OH + R_{-H}{=}O + O_2} \quad (2b)$$

$$\rightarrow \mathrm{ROH + R'_{-H}{=}O + O_2} \quad (2c)$$

$$\rightarrow \mathrm{ROOR' + O_2} \quad (2d)$$

Generally, when R = R', the rate of Reaction 2 decreases as the substitution of the peroxy radical increases, and increases with the addition of a hydroxy or acyl substituent.[11] Although this trend has been observed for self-reactions, the relationship between the kinetics of cross-reactions (R $\neq$ R') and self-reaction rates of the constituent peroxy radicals (RO_2 and R'O_2) remains poorly characterized.

The branching to the various products of Reaction 2 remains uncertain and has been the focus of substantial recent research. Most notably, it was previously widely accepted that Reaction 2d was negligible, as the resulting accretion products were not observed in laboratory oxidation studies and the proposed formation mechanism, involving an intersystem crossing, appeared unfavorable.[7,15,16] However, several recent studies have reported the formation of dimers in various oxidation systems. While some of these dimers are esters formed in the particle-phase[17] or via other gas-phase accretion mechanisms,[18] several of these products observed with chemical ionization mass spectrometry (CIMS) have masses consistent with the formation of the ROOR and are reported to form at appreciable rates that even approach

the collision rate.[19–22] The formation of the ROOR is atmospherically significant both because it terminates the radical cycle (at least temporarily) and because these products have low volatilities and are likely to play a role in the formation of secondary organic aerosol (SOA). In fact, these compounds have been observed in the remote ambient environment in both the gas- and the particle-phase, demonstrating the role that these dimers play in particle formation.[23] Additionally, a possible fourth pathway for Reaction 2 leading to an alkoxy radical, carbonyl, and HO_2 was proposed for the self-reaction of the hydroxy ethyl peroxy radical,[24] further highlighting the need for additional study of the self-reaction for a variety of peroxy radical precursors.

Recently, accrection product formation has been reported for the self-reactions of ethyl peroxy,[25] hydroxy ethyl peroxy,[24] and propyl peroxy radicals,[26] with branching fractions of 10($\pm$5)%, 23($\pm$5)%, and 10($\pm$5)% respectively. In each of these studies, the identity of the dimers was confirmed to be the ROOR formed in Reaction 2d by either gas chromatography or vacuum ultraviolet (VUV) photoionization mass spectrometry.

Despite these recent insights into the formation of accretion products via peroxy radical self- and cross-reactions, these studies have only been conducted for a limited number of peroxy radical precursors. There have been no studies that have systematically examined the relationship between the rate of accretion product formation and peroxy radical structure. However, it is necessary to probe this relationship to predict the formation rate of the accretion product for the wide variety of peroxy radicals present in the atmosphere.

In this study, we begin to fill this gap by expanding on our previous study of the formation of the accretion product in ethene-derived hydroxy peroxy radical systems.[24] Specifically, we show that the accretion product forms in a variety of small-alkene-derived peroxy radical systems and measure the formation rate of the accretion product in each of these oxidation systems relative to the formation rate of the ethene-derived accretion product. By measuring this rate in the propene, methylpropene, and cis-2-butene oxidation systems, we examine the relationship between accretion product formation and structure for these small alkene

systems. Using literature values for these rate constants where available, we further estimate the branching to the accretion product in each of these systems.

Methods

Experimental Design

In this study our goal is to quantify the formation of the peroxide accretion product for a series of small alkene-derived peroxy radicals. In each case, the peroxy radicals of interest are formed by the addition of OH to the parent alkene, followed by the rapid addition of O_2 to form the peroxy radical:

$$\mathrm{R{=}R + OH \xrightarrow{O_2} RO_2} \tag{3}$$

In all of our experiments, OH was generated by the photolysis of H_2O_2 (Reaction 4) via the illumination of eight Sankyo Denki G40T10 254 nm lamps for an average of 2 minutes. The photolysis rate of H_2O_2 under these conditions in our 800 liter FEP Teflon environmental chamber has been previously measured to be $3.0(\pm 0.5)\times 10^{-4}$ s^{-1}.[24]

$$\mathrm{H_2O_2 \xrightarrow{h\nu} OH + OH} \tag{4}$$

In several of the experiments reported here, the fraction of alkene reacted over the photolysis period was estimated by simultaneously observing the formation of glycholaldehyde in the reaction of ethylene glycol with OH (Reaction 5).

$$\mathrm{HOCH_2CH_2OH + OH \longrightarrow HOCH_2CH(O) + HO_2} \tag{5}$$

The currently recommended value for the reaction of ethylene glycol with OH is 1.45×10^{-11} cm^3 $molecule^{-1}$ s^{-1} ($\Delta \log k = \pm 0.20$).[27] In experiments where ethylene glycol was used

as a probe of the OH exposure, approximately 20-70 ppb of ethylene glycol was injected. The OH exposure was then calculated using the measured production rate of glycolaldehyde from a known concentration of ethylene glycol. This calculation yielded estimated OH exposures ranging between 0.4×10^9-6.0×10^9 molecules cm^{-3} s across the various alkene systems and conditions used here. In these systems, the OH exposure was also calculated using our photochemical box model, and values agree within a factor of 2. Therefore, in experiments in which no OH probe was used, the photochemical box model was used to estimate the fraction of reacted alkene.

We performed a suite of experiments to quantify the product of the self-/cross-reaction rate coefficient (k_2) times the branching fraction leading to accretion products (α_{2d}) of many RO_2 + R'O_2 reactions relative to the value measured for ethene in our previous work ($k_2\alpha_{2d} = 5.5(\pm2.6) \times 10^{-13}$ cm^3 molecule^{-1} s^{-1}).[24] We oxidized mixtures of ethene with propene, 2-methylpropene, or cis-2-butene and observed the formation of accretion products from all combinations of the resulting RO_2 + R'O_2 reactions. To estimate $k_2\alpha_{2d}$, experiments were performed under conditions where most ($> 90\%$) of the peroxy radicals react with HO_2 via Reaction 1a to form ROOH. Under these conditions, the ratios of the observed concentrations of ROOH provide a constraint on the ratios of the parent RO_2 concentrations (Equation 6):

$$\frac{[RO_2]_{HC}}{[RO_2]_E} = \frac{[ROOH]_{HC} k_{1,E} \alpha_{1a,E}}{[ROOH]_E k_{1,HC} \alpha_{1a,HC}} \tag{6}$$

where HC = non-ethene hydrocarbon, E = ethene, $k_{1,E}$ and $k_{1,HC}$, are the rate coefficients of Reaction 1 for ethene and non-ethene hydrocarbons, respectively, and $\alpha_{1a,E}$ and $\alpha_{1a,HC}$ are the branching fractions to ROOH. According to our photochemical box model, Equation 6 is accurate to within 7% under the conditions of our experiments.

To ensure that the $[HO_2]/[RO_2]$ ratio satisfies this condition, we add sufficient concentrations of methanol such that the reaction of OH with methanol exceeds the reaction of OH with the alkenes, as has been described previously.[24] In the oxidation experiments peformed

in this study, the relative concentrations of methanol and parent hydrocarbon yielded steady state $[HO_2]/[RO_2]$ ratios above 2.0 (as estimated by our box model). Because the rate coefficients for the reaction of RO_2 with HO_2 (k_1) are more than an order of magnitude faster than the rate coefficients of the self- and cross-reactions (k_2) for the systems studied here, the requirement that the peroxy radicals react overwhelmingly with HO_2 is satisfied under these conditions.

A measurement of $k_2\alpha_{2d}$ for each alkene can then be obtained from the measured ratio of the accretion product of interest to the ethene-derived accretion product. For the self-reaction of a given isomer of a peroxy radical derived from a non-ethene hydrocarbon (in this case propene, methylpropene, or cis-2-butene), the $k_{2,HC}\alpha_{2d,HC}$ value is given by Equation 7, where the ratio of the RO_2 concentrations is obtained from Equation 6:

$$k_{2,HC}\alpha_{2d,HC} = k_{2,E}\alpha_{2d,E}\left(\frac{[RO_2]_E}{[RO_2]_{HC}}\right)^2\left(\frac{[ROOR]_{HC}}{[ROOR]_E}\right) \tag{7}$$

If the accretion product of interest is formed via the cross-reaction of two different isomers of the same non-ethene hydrocarbon (HC_a and HC_b), this equation becomes:

$$k_{2,HC_{a,b}}\alpha_{2d,HC_{a,b}} = k_{2,E}\alpha_{2d,E}\left(\frac{[RO_2]_E}{[RO_2]_{HC_a}}\right)\left(\frac{[RO_2]_E}{[RO_2]_{HC_b}}\right)\left(\frac{[ROOR]_{HC_{a,b}}}{[ROOR]_E}\right) \tag{8}$$

Finally, for determination of the $k_2\alpha_{2d}$ value for the cross-reaction between an isomer of a non-ethene hydrocarbon and ethene, Equation 7 reduces to:

$$k_{2,HC+E}\alpha_{2d,HC+E} = k_{2,E}\alpha_{2d,E}\left(\frac{[RO_2]_E}{[RO_2]_{HC}}\right)\left(\frac{[ROOR]_{HC+E}}{[ROOR]_E}\right) \tag{9}$$

Using Equations 7-9, we calculate the $k_2\alpha_{2d}$ values for all of the self- and cross-reactions of the peroxy radical systems studied here.

Our estimate of $k_2\alpha_{2d}$ is particularly sensitive to k_1 and α_{1a}. k_1 is estimated here using the structure activity relationship (SAR) found in Wennberg et al.[14] This rate constant has

been measured for the primary peroxy radical derived via the oxidation of 2-methylpropene ($k_1 = 1.5(\pm 0.9) \times 10^{-11}$ cm^3 molecule^{-1} s^{-1})[6] and the secondary peroxy radical derived via the oxidation of cis-2-butene ($k_1 = 1.5(\pm 0.4) \times 10^{-11}$ cm^3 molecule^{-1} s^{-1}).[5] These measured values are the same as those values predicted by the structure-activity relationship within error (1.6×10^{-11} cm^3 molecule^{-1} s^{-1} at 295 K for both compounds), and so the SAR values are used in all cases for consistency.

Estimates of α_{1a} were derived from the concentration of ROOH formed in the high HO_2 experiments. In these experiments, the amount of ROOH formed divided by the concentration of the reacted alkene is approximately equal to the branching fraction to Reaction 1a (Equation 10).

$$\frac{\Delta[ROOH]}{\Delta[HC]} = \alpha_{1a,HC} \tag{10}$$

According our photochemical box model, for the conditions of our experiments, Equation 10 is accurate to better than 9%. There is additional error induced by the estimation of the reacted alkene used in the calculation of α_{1a}. In experiments where ethylene glycol was included as a probe of OH exposure, we found that the modelled and measured OH exposure agreed to within a factor of 2. Therefore, we assign the modelled OH exposures, and by extension the fraction of reacted alkene, an uncertainty of 50%. This is by far the largest source of uncertainty in the estimation of α_{1a}. Further, this error is much larger than that induced by the uncertainties in the values of k_1. Therefore, we assign the α_{1a} an uncertainty of 50% and the overall calculation of $k_2\alpha_{2d}$ a corresponding uncertainty of 50%.

Finally, to assist in assigning the different ROOR isomers in the gas chromatograms, we performed experiments where we did not add methanol in order to maximize the fraction of RO_2 undergoing self- and cross-reactions and thus the signal-to-noise ratios of the resulting chromatograms. These experiments are labeled 'high RO2' in the discussion below and generally contained $[HO_2]/[RO_2]$ ratios that were much less than 1.

Instrumentation

All measurements in this study were conducted using the Caltech gas chromatograph chemical ionization mass spectrometer (GC-CIMS). This instrument has been described in detail previously,[28] but a brief description is given here.

The Caltech high-resolution time-of-flight chemical ionization mass spectrometer (HRToF-CIMS) uses CF_3O^- as a reagent ion, which is produced via the interaction of dilute CF_3OOCF_3 gas in N_2 with polonium-210. In direct sampling mode, the analyte gas is sampled at approximately 2000 sccm, and 180 sccm of this sample passes through a Teflon-coated metal frit into a Teflon-coated glass flow tube that is maintained at a pressure of approximately 35 mbar. Here, the sample is diluted with N_2 and turbulently mixes with the 380 sccm flow of N_2 from the ion source. The analytes are then ionized by reaction with the reagent ion. For most of the compounds considered here, the analyte forms a cluster with the reagent ion that appears at a mass-to-charge ratio of the molecular weight of the compound plus the mass of CF_3O^- (m/z = mw + 85). However, analytes may also undergo a fluorine transfer reaction, thus appearing at a mass-to-charge ratio equal to the molecular weight of the analyte plus the mass of fluorine (m/z = mw + 19). Although fragmentation in this ionization scheme is minimal compared to the fragmentation observed in other chemical ionization schemes, some compounds still lead to characteristic fragments. For example, organic hydroperoxides characteristically form fragment ions at m/z 63 and m/z 81.[29–31] The ionized analytes are then directed into the mass spectrometer through a pinhole and a conical hexapole ion guide, where they are subsequently detected. Signals were collected for mass-to-charge ratios between m/z 19 and m/z 396, and the mass resolving power of the instrument is approximalely 3000 m/Δm.

The metal-free, low-pressure gas chromatograph consists of a 2-meter silica-coated column that is cooled via the expansion of liquid CO_2 and heated with resistance heaters. During GC sampling in these experiments, the analyte gas was sampled at approximately 1200 sccm and diluted via the addition of a nitrogen flow perpendicular to the sample flow. The diluted

sample was then collected in a small trap prior to the column at -10°C, -20°C, or -30°C for approximately 2-10 min, with the chosen trapping temperatures, dilution factors, and trapping times chosen to maximize the concentration of analyte trapped while avoiding the trapping of water or loss of reagent ion. After trapping, the temperature was increased to 130°C at a pre-determined ramping rate with 5 sccm of nitrogen flowing through the column. The effluent was then directed into the flow tube with a 200 sccm pickup flow of nitrogen and detected by the HRToF-CIMS. The HRToF-CIMS can readily be switched to sample from the GC or directly from the chamber. A complete list of the temperature ramps and trapping conditions used in these experiments is given in the SI. For each experiment, a background chromatogram was taken prior to the initiation of oxidation and three chromatograms were taken after the oxidation period.

CIMS Calibration and GC Collection and Transmission Efficiencies

The sensitivity of the CIMS to most compounds in this study was estimated using the sensitivities of chemically similar compounds. In prior work, we measured a sensitivity of $2.5(\pm 0.2) \times 10^{-4}$ cts/pptv of the CIMS to ethylene glycol.[24] The sensitivities of the other RO_2 reaction products were then estimated via calculation of their ion-molecule collision rates relative to that of ethylene glycol. This procedure is described in detail in previous work,[24] but is briefly summarized here. The CIMS instrument used in this work implements a transverse ionization scheme that results in a short interaction time (approximately 5 ms) between the analyte and reagent ions. In this implementation, the sensitivity of the analyte is approximately proportional to the ion-molecule collision rate, the fraction of these collisions that result in ionization of the analyte, the transmission efficiency of the resulting ions, and any fragmentation of the analyte in the ionization process. Further, this sensitivity also depends on the total number of reagent ions (which includes CF_3O^- and its clusters with water and H_2O_2) - since the fraction of reagent ions reacting with analytes is low, we can normalize the analyte signals to the total reagent ion signal. Specifically, to remain in

a linear counting regime, we normalize our signals to the sum of the signals of the isotopic analogues of the reagent ions (m/z = 86, 104, and 120). The resulting signals are then proportional to the concentration of the analyte in the sample.

CF_3O^- binds particularly strongly to multifunctional organic compounds,[32] and so the fraction of the analyte that undergoes ionization generally depends on the ion-molecule collision rate. For analytes that form weakly bound clusters (such as H_2O_2), not every collision results in the formation of a stable ion cluster. Such analytes are generally identified by probing the relationship between the sensitivity and the temperature and humidity, as the sensitivity of these compounds tends to exhibit a negative dependence of temperature and a complex dependence on water concentration.[33] The efficiency of cluster formation following collision may also decrease due to fragmentation of the analyte. In our previous work on the ethene-derived peroxy radical self-reaction, we found that the clusters of the resulting RO_2 products with the reagent ion were well bound and exhibited little fragmentation. Due to the similar sizes and chemical structures of the compounds studied here compared to those probed in the prior study, we assume that the compounds considered in this study are similarly well-bound and thus that their sensitivities will scale with their ion-molecule collision rates. The sensitivities of the compounds measured in this study are then estimated by calculating their ion-molecule collision rates relative to ethylene glycol and using this scaling factor to obtain the sensitivity from the measured ethylene glycol sensitivity. The calculated ion-molecule collision rates relative to ethylene glycol are given in the SI and are obtained using the methods outlined in Su et al[34] and quantum calculations of the dipole moments and polarizabilities of the relevant compounds.[35] Where quantum calculations of polarizabilities and dipole moments were not available, the sensitivity of the compound was assumed to be the same as the most chemically similar compound for which the ion-molecule collision rate was available.

The GC collection and transmission efficiencies for each compound were determined by comparison of the sum of the total GC signal to the average CIMS signal. The collection and

transmission efficiencies ranged between 10% and 100% - the lowest values generally reflect small ketones and alcohols for which the trapping was inefficient. The average transmissions of each of the relevant compounds is given in the SI.

Isomer Distribution and Peak Fitting

The calculations of the self- and cross-reaction rate constants for the individual isomers of the various peroxy radicals required the separation of the various isomers of the resulting RO_2 products in the gas chromatograph and the subsequent quantification of their concentrations. The relative concentrations of each of these isomers was determined by fitting each peak using a modified open-source MATLAB peak-fitting function.[36] These GC peaks are best fit in our instrument to an exponentially-broadened Gaussian with varying peak widths and exponential time constants. The peak widths and time constants that minimized the total error for these fits were determined by performing a bootstrap best-fit procedure in which 1,000-10,000 trials were performed with the parameters randomly varied in a range equal to $\pm$50% of the initial guess. The resulting best-fit parameters, which are provided in the SI for the experiments discussed here along with the errors and R^2 values of the fits, were then used to calculate the area under each chromatgraphic peak.

To account for transmissions and trapping efficiencies less than unity in the GC, we did not calculate the concentration of each isomer directly from this integrated GC signal. Rather, the relative proportion of each compound was calculated using the ratio between the calculated areas and these proportions were subsequently multiplied by the total signal in the CIMS to determine the concentrations of each isomer. In this calculation, we implicitly assume that the direct sampling signal represents the total concentration of a given set of isobaric isomers and that the trapping and transmission efficiencies of these different isomers are the same.

Reagent Preparation

H_2O_2 (30% by mass, Macron Fine Chemicals) was measured by weight into a pre-weighed three-way glass vial and injected into the chamber by evaporating this weighed sample with dry air flowing at 20 SLM. The glass vial was reweighed following injection to ensure complete evaporation of the sample. Ethylene glycol (Sigma-Aldrich) was injected in a similar manner, with the glass vial partially immersed in warm water to ensure evaporation of the sample.

Ethene ($\geq$ 99.5%, Sigma-Aldrich), methanol ($\geq$ 99.9%, Sigma-Aldrich), 2-methylpropene (99%, Sigma Aldrich), cis-2-butene ($\geq$ 99%, Sigma Aldrich), and propene ($\geq$ 99%, Sigma Aldrich) samples were measured into 500-mL glass bulbs via a manometric system in which the bulb was attached simultaneously to a vacuum/N_2 system and to the reagent source. The desired concentration of the relevant hydrocarbon was then obtained by serial dilution with pressure measurements conducted using pressure sensors (MKS 1000 and 10 Torr baratron pressure transducers). The purity of the samples and the concentrations measured using manometry were confirmed by taking IR spectra in a 19 cm pyrex FTIR cell with CaF_2 windows and fitting the resulting spectra to cross sections obtained from the PNNL IR Database.[37] The measurements taken with manometry and the concentration calculated from the FTIR spectra agree to within 30%.

Results and Discussion

2-Methylpropene

The expected products of the NO_x-free OH-initiated oxidation of 2-methylpropene are shown in Scheme 1. Two peroxy radical isomers, a tertiary peroxy radical (3-MP) and a primary peroxy radical (1-MP), are formed via the major and minor OH addition reactions, respectively. Hydrogen abstraction has been found to account for <5% of the overall reaction of 2-methylpropene with OH and is therefore neglected in this analysis.[1,38] Representative

chromatograms of the major accretion and hydroperoxide products are given in Figure 1.

In experiments with high HO_2/RO_2 ratios ($\frac{HO_2}{RO_2} > 2$), the isomeric distribution of the ROOH products is expected to reflect the ratio of the production rates of the peroxy radical isomers, due to the observed lack of dependence of k_1 on peroxy radical structure.[14] In these high HO_2 experiments, the average distribution of 1-MP-ROOH/3-MP-ROOH is 16(±1)%/84(±1)%. This is within 5% of the distribution found by Teng et al. (21(±2)%/79(±2%)),[38] further confirming that the primary loss of RO_2 in these experiments is reaction with HO_2.

In the high RO_2 regime ($\frac{HO_2}{RO_2} << 1$), the fraction of 1-MP-ROOH is significantly lower than that observed in the high HO_2 condition, with an average isomer distribution of 3(±1)% 1-MP-ROOH and 97(±1)% 3-MP-ROOH. Under these conditions, the ROOH isomer distribution is significantly altered by the loss rates of 3-MP and 1-MP RO_2 due to self- and cross-reaction chemistry. The dramatic decrease in the production of 1-MP-ROOH relative to 3-MP-ROOH is consistent with previous observations that the rate of self- and cross-reactions of primary peroxy radicals are rapid compared to those of tertiary peroxy radicals.[11]

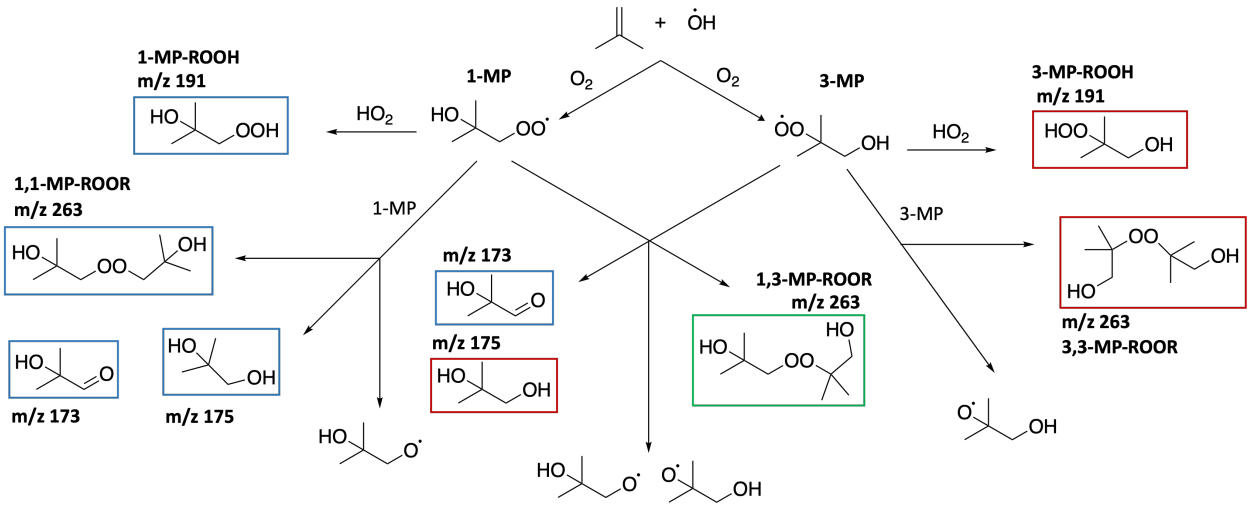

Scheme 1: Reaction scheme for the oxidation of 2-methylpropene by OH. Stable products that can be observed with the CF_3O^- GC-CIMS are boxed and color-coded such that products that are derived from the primary peroxy radical are in blue, those derived from the tertiary peroxy radical are in red, and products formed from the cross-reactions of the primary and tertiary peroxy radicals are in green. Each product is labelled with the m/z of that product in our CIMS, which is equal to the molecular weight + 85. In the presence of O_2, the alkoxy radicals shown will decompose to formaldehyde and acetone.

The isomer distribution of the methylpropene-derived accretion product formed in Reaction 2 is influenced by the competing factors of peroxy radical abundance and reaction rate. Although the branching to the formation of tertiary peroxy radicals in the OH-initiated oxidation of 2-methylpropene is approximately 80%,[38] the self-reactions of tertiary peroxy radicals are generally several orders of magnitude slower than those of primary peroxy radicals.[7,11] In the high RO_2 condition three isomers at the mass of the accretion product (m/z 263) are observed, consistent with the expected products outlined in Scheme 1. Therefore, we see that the accretion product is formed at appreciable rates in all three of the possible self- and cross-reactions observed in this oxidation system.

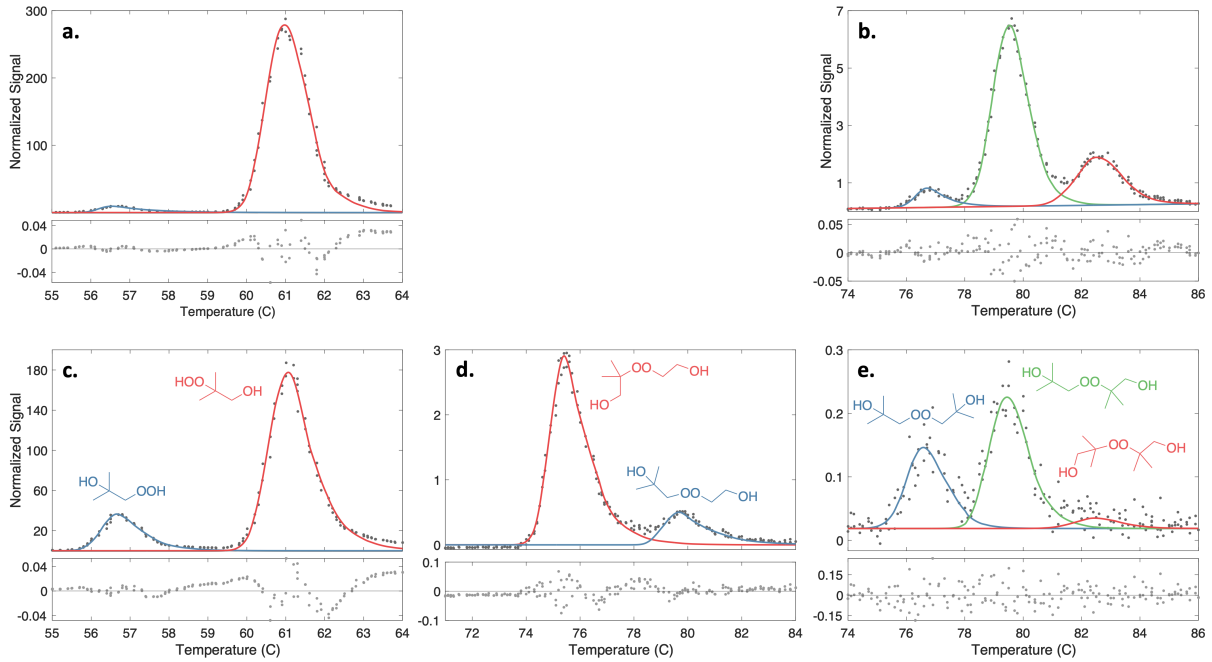

Figure 1: Representative chromatograms of ROOH (a. and c.) and ROOR (b., d., and e.) products formed in the high RO_2 (upper panel) and high HO_2 (lower panel) oxidation of 2-methylpropene. Experiments represented in the lower panel also included ethene. The experimentally measured signal is given as dark gray dots, while the colored lines are the bootstrap best fits of the chromatographic data. The corresponding structures are the suggested assignments of these peaks. Below each chromatogram are plots of the residuals of the best fits given as fractions of the maximum peak value.

The peak assignments given in Figure 1 follow the observation that, in the Caltech GC-CIMS instrument, compounds with primary -OH groups elute at higher temperatures than those with tertiary -OH groups due to the corresponding decrease in interaction strength between the analyte and the column.[39] The ROOR produced in the cross-reaction of 1-MP and 3-MP (1,3-MP-ROOR) is produced in the highest proportion, constituting on average 69(±4)% of the total concentration of methylpropene-derived accretion products. That formed in the self-reaction of 3-MP (3,3-MP-ROOR) constitutes 23(±3)% of this signal, with 7(±2)% of the signal on average attributed to the peroxide formed in the self-reaction of 1-MP (1,1-MP-ROOR). Clearly, the cross-reaction between 1-MP and 3-MP is favored over the self-reaction of 3-MP. However, the 1-MP reacts quickly such that the steady state

concentration of 1-MP is quite low and a significant concentration of 3,3-MP-ROOR is formed despite the slow self-reaction rate constant of tertiary peroxy radicals. These observations are further quantified and discussed in the section on ROOR formation rates below.

In experiments with high HO_2/RO_2 ratios, 2-methylpropene and ethene were oxidized together to measure the relative production rates of the ethene- and methylpropene-derived accretion products, as described in the Methods section. Under these conditions, the proportion of 3,3-MP-ROOR decreases appreciably to between 0-5% of the total methylpropene-derived ROOR concentration. The signal-to-noise ratio of this peak is very low, with the peak indistinguishable from the noise in some cases - therefore, significant uncertainty is assigned to this fitted peak area. On the other hand, the concentrations of 1,1-MP-ROOR and 1,3-MP-ROOR are comparable, with average proportions of 37(±1)% and 61(±2)%, respectively. Further, two compounds are observed at m/z 235, consistent with accretion products formed in the cross-reactions of 2-methylpropene and ethene-derived peroxy radicals (E-1-MP-ROOR and E-3-MP-ROOR). These compounds are produced in unequal proportions, with a distribution of 78(±3)%/22(±3)%. The observed decrease in the concentrations of 3,3-MP-ROOR and 3,1-MP-ROOR relative to 1,1-MP-ROOR in the presence of ethene suggests that 3-MP preferentially reacts with ethene-derived peroxy radicals over reaction with 1-MP or 3-MP. We thus assign the more prominent peak at m/z 235 to E-3-MP-ROOR. Once again, these observations will be discussed and quantified further in the section on ROOR formation rates.

Cis-2-Butene

The simplified mechanism of the NO_x-free OH-initiated oxidation of cis-2-butene is given in Scheme 2. Once again, stable products that can be observed via clustering with CF_3O- in the Caltech GC-CIMS are boxed and labelled with the corresponding m/z. The H-abstraction pathway is once again expected to be negligible (<5% of the total reaction with OH). In contrast to the 2-methylpropene system, the symmetry of the parent molecule yields only one

possible structural isomer of the peroxy radical. However, three stereoisomers of the peroxy radical (two enantiomers and a meso compound) are possible, and these will react to form distinct ROOH, ROOR, and diol products that have the potential to be chromatographically separated (for simplicity, stereoisomers are not shown in Scheme 2). Representative chromatograms of the resulting peroxide, hydroperoxide, and diol products are given in Figure 2.

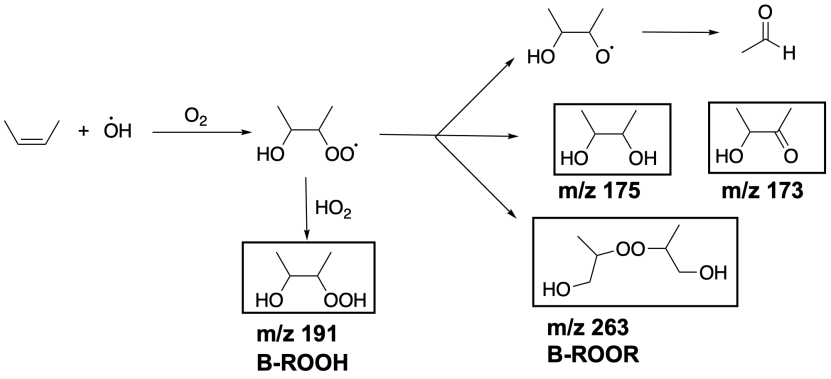

Scheme 2: Reaction scheme for the oxidation of cis-2-butene by OH in the presence of O_2. Stable products that can be observed with the CF_3O^- GC-CIMS are boxed and labelled with the m/z at which they are observed. For simplicity, stereosiomers are not included.

As described above, three stereosiomers of the peroxy radical are generated, the reactions of which are expected to produce multiple stereoisomers of the resulting B-ROOH, B-ROOR, and 2,3-butanediol products. In agreement with this expectation, two closely separated peaks are observed in the chromatogram at m/z 175, the mass-to-charge ratio at which 2,3-butanediol appears in the CIMS, with a distribution of 34(±8)%/66(±8)% in the high RO_2 ($\frac{[HO_2]}{[RO_2]} << 1$) experiments. Comparison of this chromatogram with that of a 2,3-butanediol standard containing a mixture of stereoisomers confirms the identity of these peaks as the stereoisomers of 2,3-butanediol (see Figure S1). Due to the chemical similarity of the enantiomers, we hypothesize that one of these peaks is a mixture of the enantiomers, while the other is the meso compound. However, we cannot definitively assign these peaks at this time. In contrast, multiple peaks are not observed at the masses associated with the

ROOH and ROOR products, likely due to a lack of chromatographic separation.

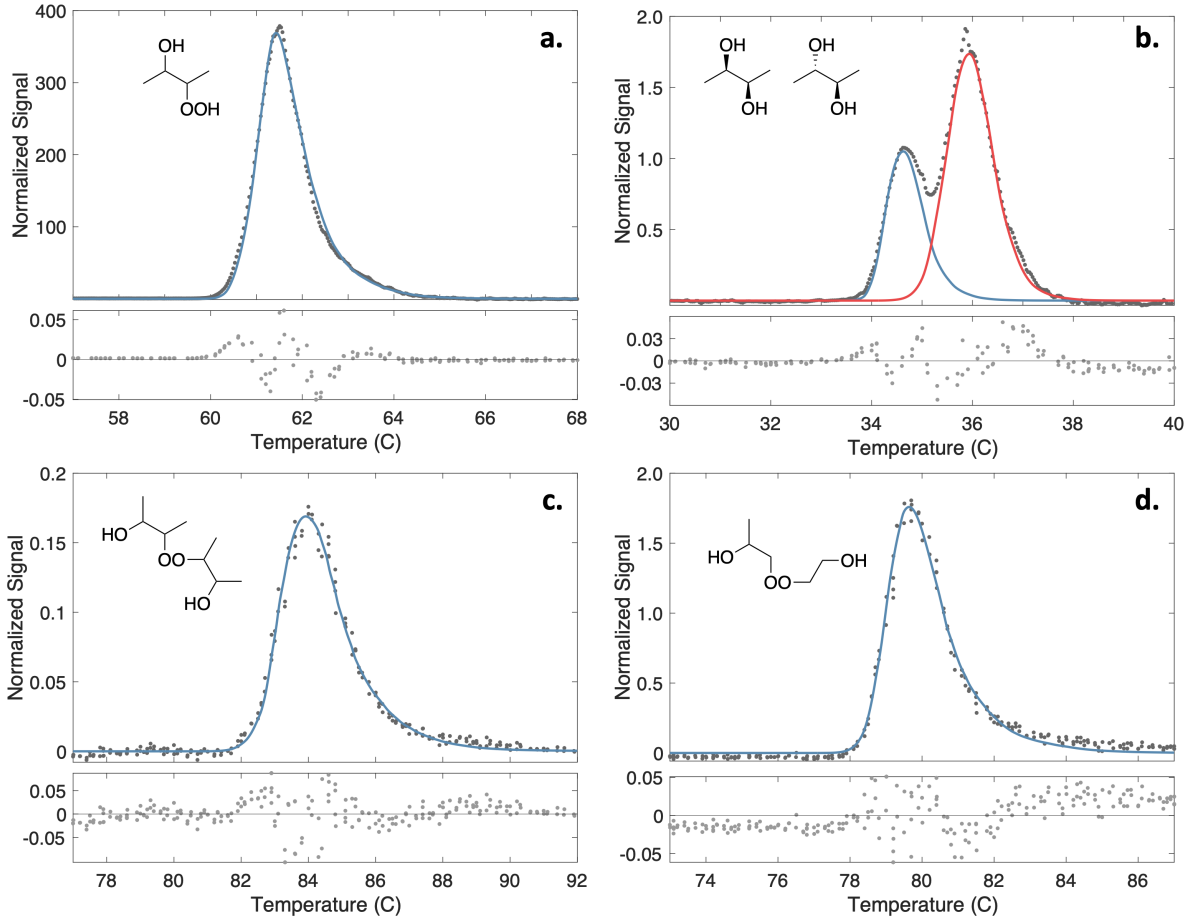

Figure 2: Sample gas chromatograms of several important masses produced in the oxidation of cis-2-butene by OH in the presence of O_2 and ethene, including (a) the ROOH, (b) the diol, (c) the ROOR formed in the self-reaction, and (d) the ROOR formed in the cross-reaction with ethene. Experimentally measured signals are given in gray dots, while the bootstrapped best fits to these peaks are given in colored lines. The provided structures correspond to the assigments of these peaks - the two structures in b. are not assigned to a particular peak. Below each chromatogram the residuals of the best fits are plotted as a fraction of the maximum peak signal. The chromatograms in a. and b. are corrected for significant tailing - this correction is described in the SI.

As in the analysis of the 2-methylpropene system, high HO_2 experiments ($\frac{[HO_2]}{[RO_2]} > 2$) were performed with a mixture of ethene and cis-2-butene to directly compare the formation rates of the accretion products. The distribution of the stereosiomers of butanediol does not change (within error) under this condition, with an average distribution of

31(±6)%/69(±6)%. Without chromatographic separation of the stereoisomers of the ROOH products, it is difficult to draw any definitive conclusions from this observation of the butanediol isomeric distribution. In these experiments, accretion products formed in the cross reactions between the ethene- and cis-2-butene-derived peroxy radicals (m/z 235) were observed alongside accretion products resulting from the corresponding self-reactions (m/z 263), as shown in Figure 2d and 2c, respectively. The measured formation rates of these compounds will be discussed in the section on ROOR formation rates.

Propene

The mechanism of the OH-initiated NO_x-free propene oxidation system is given in Scheme 3. Two structural isomers of the propene-derived hydroxyperoxy radical are generated in the reaction of propene and OH - a primary peroxy radical (1-P) via the minor addition pathway and a secondary peroxy radical (2-P) in the major addition pathway. Similarly to the methylpropene system, at sufficiently high HO_2/RO_2 concentrations ($\frac{HO_2}{RO_2} > 2$) the distribution of the ROOH isomers is expected to match that of the peroxy radical isomers. This is consistent with the measured isomer distribution in the high HO_2 experiment, with an observed distribution of 35%/65% for 1-P/2-P, which is within 5% of the previously measured distribution (40(±3)%/60(±3)% for 1-P/2-P).[38]

This distribution diverges from the relative production of the peroxy radical isomers in experiments with high RO_2/HO_2 ratios ($\frac{[HO_2]}{[RO_2]} << 1$), exhibiting a distribution of 16%/84%. This perturbation demonstrates, as expected, that the primary peroxy radical undergoes self- and cross-reaction more quickly than the secondary peroxy radical. However, this perturbation is less substantial than that observed for the distribution of 1-MP-ROOH and 3-MP-ROOH, suggesting that the difference in self- and cross-reaction rates between the tertiary and primary peroxy radicals is more significant than that between the secondary and primary peroxy radical. This is consistent with previous observations that the reactivity with respect to self- and cross-reaction decreases with increasing peroxy radical substitution.

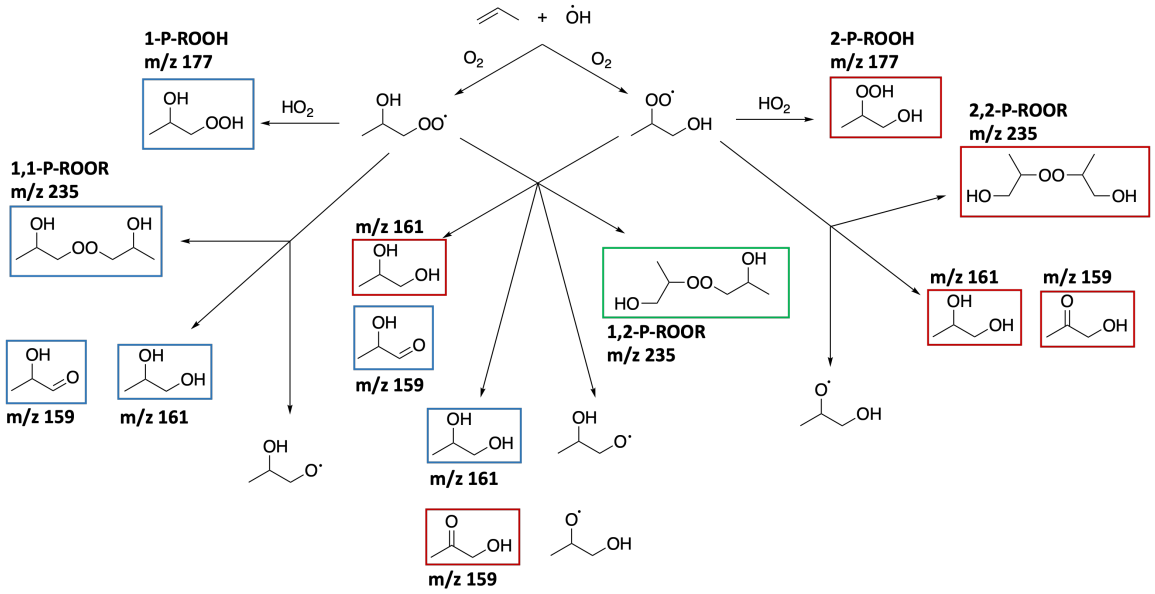

Scheme 3: Reaction scheme for the oxidation of propene by OH in the presence of O_2. Stable products that can be observed with the CF_3O^- GC-CIMS are boxed and color-coded such that products that are derived from the primary peroxy radical are in blue, those derived from the secondary peroxy radicals are in red, and products formed from the cross-reactions of the primary and secondary peroxy radicals are in green. Each products is labelled with the m/z of that product in our CIMS, which is equal to the molecular weight + 85. In the presence of O_2, the alkoxy radicals will form formaldehyde and acetaldehyde.

As in the methylpropene oxidation system, the isomer distribution of the propene-derived accretion products (1,1-P-ROOR, 1,2-P-ROOR, and 2,2-P-ROOR) is influenced by the competing effects of the peroxy radical distribution and the self- and cross-reaction rates. However the differences in these quantities across the peroxy radical isomers are less pronounced in the propene system than in the 2-methylpropene system. In experiments with high RO_2/HO_2 ratios, the accretion product formed in the cross-reaction of the primary and secondary peroxy radicals is most prominent, and is present in an average proportion of 56%. On the other hand, the 1,1-P-ROOR and 2,2-P-ROOR compounds are present in similar proportions, with an average distribution of 26%/18%.

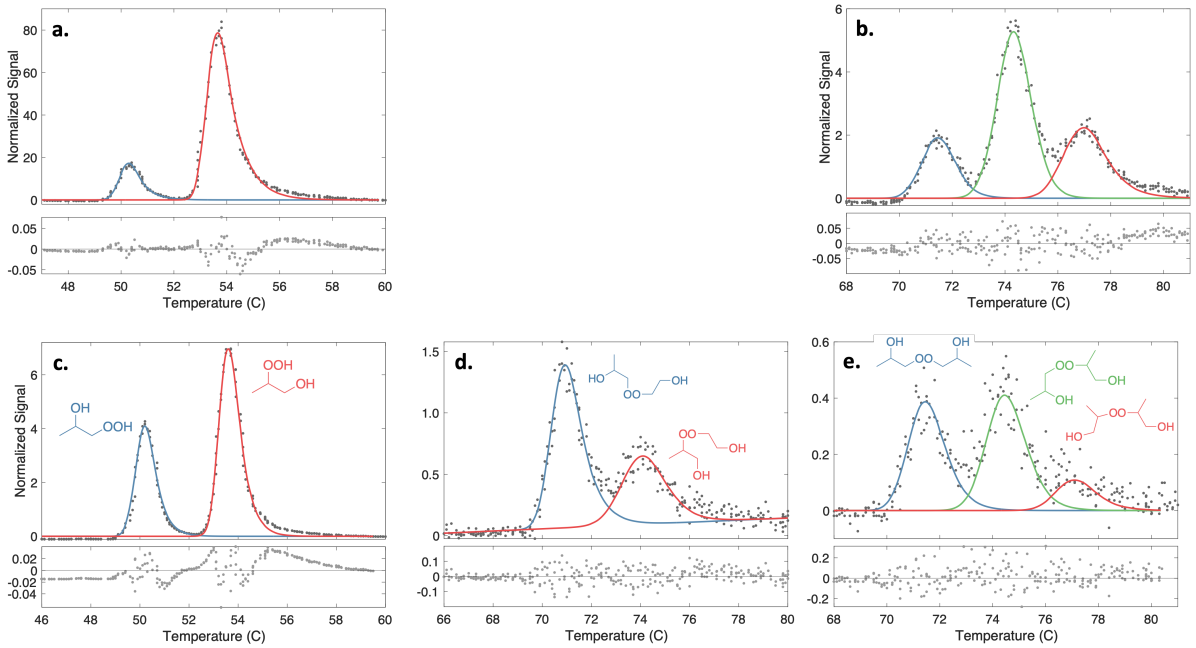

Figure 3: Sample gas chromatograms of several important masses produced in the oxidation of propene by OH in the presence of O_2 and ethene, including the ROOH (a and c), the ROOR formed in the self-reaction (b and e), and the ROOR formed in the cross-reaction with ethene (d). Chromatograms in the upper panel (a and b) are from experiments with high RO_2/HO_2 ratios, while those in the lower panel (c, d, and e) are from experiments with high HO_2/RO_2 ratios. The bootstrapped best-fits of the relevant peaks are plotted on top of the GC traces, and structures are given for the assignments of these peaks. Below each chromatogram the residuals of the best fits are plotted as fractions of the maximum peak signal.

In the high HO_2 system, the proportion of the total ROOR signal that is composed of 2,2-P-ROOR decreases to 11($\pm$2)% on average. This is an effect similar to that observed in the high HO_2 regime of the 2-methylpropene system, in which the fraction of 3,3-MP-ROOR dramatically decreases due to the reaction of 3-MP with ethene-derived peroxy radicals. This suggests that 2-P also preferentially reacts with ethene-derived peroxy radicals over reaction with 1-P or 2-P, although this difference between reactivity in the cross-reaction vs. the self-reaction is less pronounced than that observed for the tertiary peroxy radical. Further, two peaks are observed at the mass of an accretion product formed in the cross-reaction of ethene-derived peroxy radicals and propene-derived peroxy radicals (m/z 221). These are

produced with an average distribution of 63%/37%. In analogy to 1,3-MP-ROOR, due to the observed decrease in the production of 2,2-P-ROOR under these conditions, we assign the more prominent peak to 2P-E-ROOR. The production rates of these and other peroxy radicals are quantified and discussed further in the next section.

ROOR Formation Rates

The formation rates of the various accretion products formed in these alkene oxidation systems ($k_2\alpha_{2d}$) were measured relative to the formation rate of the ethene-derived accretion product, as described in the Methods section. The resulting $k_2\alpha_{2d}$ values for the self- and cross-reactions of the various peroxy radical isomers formed in the 2-methylpropene, propene, and cis-2-butene oxidation systems (and the relevant cross-reactions with ethene) are given in Table 1.

In Figure 4, the measured $k_2\alpha_{2d}$ values for each of the self-reactions are plotted as a function of carbon number of the peroxy radical and color-coded by peroxy radical substitution. Despite the uncertainties in our measurements, it is clear that the formation rate of the accretion product decreases by approximately an order of magnitude as the substitution of the peroxy radical increases, with the formation of the ROOR being the fastest for primary peroxy radical self-reactions (on the order of 10^{-13} cm^3 molecule^{-1} s^{-1}) and the slowest for the tertiary peroxy radical self-reaction (on the order of 10^{-15} cm^3 molecule^{-1} s^{-1}). This observation is consistent with the general observation that the overall rate of the self-reaction decreases with increasing peroxy radical substitution[7,11] and suggests that, at least for small alkene-derived peroxy radicals, $k_2\alpha_{2d}$ depends strongly on peroxy radical substitution with a smaller dependence on carbon number. The data further suggest that there is a decrease in ROOR formation with increasing carbon number, with $k_2\alpha_{2d}$ decreasing by a factor of 1.45 with each increasing carbon for primary RO_2 and decreasing by a factor of 1.2 across the C3 and C4 secondary peroxy radicals. However, these factors are within the uncertainties of our measurements, and this relationship should be investigated further.

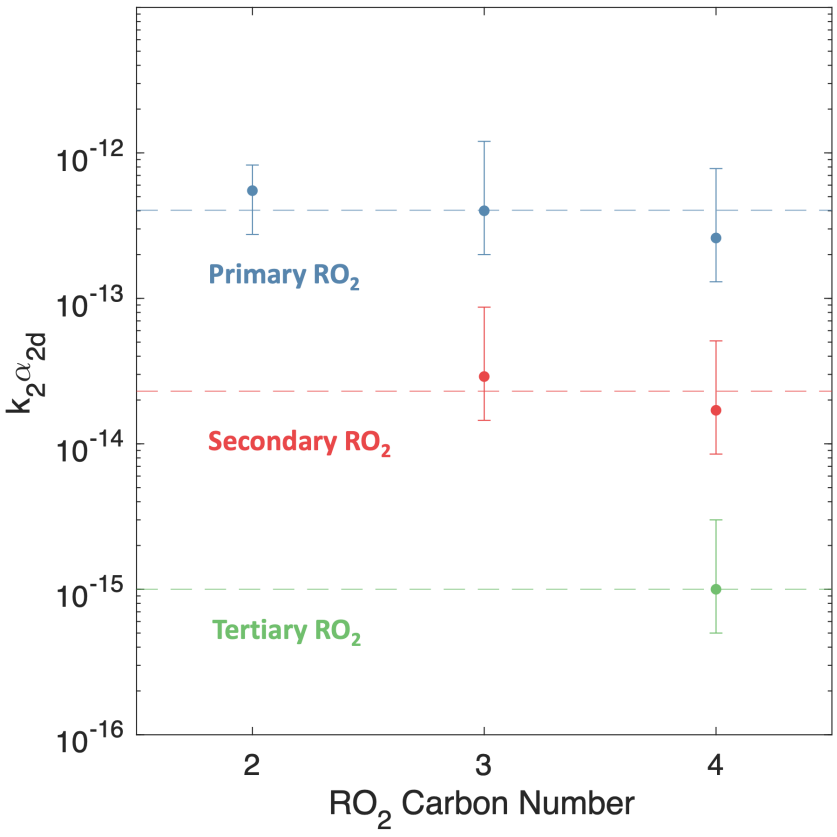

Figure 4: Measured values of $k_{RO_2+RO+2}\alpha_{ROOR}$ for the self-reactions of the ethene, methylpropene, propene, and cis-2-butene-derived peroxy radical systems, plotted as a function of carbon number of the peroxy radicla and colored by substitution of the peroxy radical. Dashed lines give the average value of $k_{RO_2+RO+2}\alpha_{ROOR}$ for each of the primary, secondary, and tertiary peroxy radical groups.

Of the systems studied here, the self-reaction rate constants for the reactions of the 2-B,[5] 1-MP,[6,40] and 3-MP peroxy radicals[41] have been measured in prior studies. For these systems, we use the $k_2\alpha_{2d}$ measured in this work and the literature value for the rate constant to estimate α_{2d}, the branching fraction to the formation of the accretion product. These values are given in the last column of Table 1. We can further estimate α_{2d} for the propene-derived peroxy radical isomers using measured rates for peroxy radicals with similar structures - these estimates are given in Table 1 as well (possible ranges for these values are discussed in more detail below). These results suggest that α_{2d} decreases with increasing carbon chain

length. The relationship between peroxy radical substitution and α_{2d} is less clear. The estimated α_{2d} values for C4 peroxy radical self-reactions, which encompass primary, secondary, and tertiary peroxy radicals, have significantly overlapping uncertainties and similar values, making interpretation of a trend impossible. The implied α_{2d} values determined for C3 peroxy radicals, which include a secondary and a primary peroxy radical, suggest that α_{2d} decreases with increasing substitution, but with only two points this trend is not certain. Clearly, further studies are needed to explore the relationship between structure and α_{2d}.

Table 1: The measured $k_2\alpha_{2d}$ values for each of the systems in this study. For those systems for which the peroxy radical self-reaction rate constant has been measured or can be estimated ($k_{2,meas}$), the literature value of the rate is given and the resulting implied α, calculated from the literature k value and the reported $k_2\alpha_{2d}$ value, is given in column 3. Additionally, α_{2d} is estimated for cross-reaction using the arithmetic mean of the self-reactions ($k_{2,ar}$).[a]All values in this column are from Murphy et al 2023.[24] [b]Jenkin and Hayman 1995.[5] The value reported in Jenkin and Hayman is given as a range of possible values between 3.9×10^{-13} $\frac{\text{molec}}{\text{cm}^3\text{s}}$ and 6.0×10^{-13} $\frac{\text{molec}}{\text{cm}^3\text{s}}$. A value in the middle of this range is reported here and used to estimate α. [c]Boyd et al 1996.[6] [d]Boyd et al 2003.[41] [e]Values estimated using measured rate constants for peroxy radicals with similar structures.

Reactants	$k_2\alpha_{2d}$ $(\times10^{-13})$ $\frac{\text{molec}}{\text{cm}^3\text{s}}$	$k_{2,meas}$ $(\times10^{-13})$ $\frac{\text{molec}}{\text{cm}^3\text{s}}$	$k_{2,ar}$ $(\times10^{-13})$ $\frac{\text{molec}}{\text{cm}^3\text{s}}$	Implied α_{2d}
Ethene				
$HOCH_2CH_2O_2$ + $HOCH_2CH_2O_2$	5.5(±2.6)[a]	24(±10)		.23(±.05)
Propene				
$CH_3CH(OH)CH_2O_2$ + $CH_3CH(OH)CH_2O_2$	4.0	24[e]		.17
$CH_3CH(O_2)CH_2OH$ + $CH_3CH(O_2)CH_2OH$	.29	5.0[e]		.06
$CH_3CH(O_2)CH_2OH$ + $CH_3CH(OH)CH_2O_2$	2.2		16	.14
$CH_3CH(OH)CH_2O_2$ + $HOCH_2CH_2O_2$	4.6		24	.19
$CH_3CH(O_2)CH_2OH$ + $HOCH_2CH_2O_2$	4.2		16	.26
cis-2-butene				
$CH_3CH(OH)CH(O_2)CH_3$ + $CH_3CH(OH)CH(O_2)CH_3$	.17	5.0(±1.1)[b]		.03(±.02)
$CH_3CH(OH)CH(O_2)CH_3$ + $HOCH_2CH_2O_2$	1.6		16(±8)	.10(±.05)
2-methylpropene				
$(CH_3)_2C(OH)CH_2O_2$ + $(CH_3)_2C(OH)CH_2O_2$	2.6	51(±34)[c]		.05(±.04)
$(CH_3)_2C(O_2)CH_2OH$ + $(CH_3)_2C(O_2)CH_2OH$	.010	.15(±.05)[d]		.07(±.04)
$(CH_3)_2C(OH)CH_2O_2$ + $(CH_3)_2C(O_2)CH_2OH$	.80		26(±19.5)	.03(±.02)
$(CH_3)_2C(OH)CH_2O_2$ + $HOCH_2CH_2O_2$	3.3		38(±30)	.08(±.07)
$(CH_3)_2C(O_2)CH_2OH$ + $HOCH_2CH_2O_2$	2.1		12(±6.4)	.18(±.13)

Although k_2 for the propene-derived peroxy radical systems have not been measured to our knowledge, we estimate a possible range for α_{2d} and k_2 for the self-reactions of 1-P and 2-P using those values measured for other peroxy radical systems. First, we assign possible maximum and minimum values for the rate constant and calculate the implied α_{2d}. As a maximum we assign a value of k_2 approximately equal to that found for the ethene-derived peroxy radical self-reaction ($k_2 = 2.4 \times 10^{-12}$ molec cm^{-3} s^{-1}). This yields estimated lower limits of the branching fractions for the self-reactions of each isomer of $\alpha_{2d,1P} = .17$ and $\alpha_{2d,2P} = .01$. Alternatively, assigning a likely low-limit value of k_2 approximately equal to that found for the cis-2-butene-derived peroxy radical yields $\alpha_{2d,1P} = 0.80$ and $\alpha_{2d,2P} = 0.06$. If we instead assume, as an upper limit, that $\alpha_{2d} = 0.23$ (equal to that of the ethene-derived peroxy radical) for both isomers, we obtain an estimate of the rate coefficient of $k_{2,1P+1P} = 1.7 \times 10^{-12}$ molec cm^{-3} s^{-1} and $k_{2,2P+2P} = 1.3 \times 10^{-13}$ molec cm^{-3} s^{-1}. Assuming a value closer to that of the cis-2-butene system ($\alpha_{2d} = 0.03$) yields a rate constant of $k_{2,1P+1P} = 1.3 \times 10^{-11}$ molec cm^{-3} s^{-1} and $k_{2,2P+2P} = 9.7 \times 10^{-13}$ molec cm^{-3} s^{-1}. Further work is clearly required to measure either the rate constant or branching fraction for the propene-derived peroxy radical system.

In addition to the formation rates of the accretion products in the self-reactions the various peroxy radical isomers of each of the alkene systems, Table 1 also reports the measured $k_2\alpha_{2d}$ values for the various cross reactions of these isomers with other isomers of the same alkene-derived peroxy radicals and with the ethene-derived peroxy radicals. The relationship between the $k_2\alpha_{2d}$ for the cross-reactions and the corresponding self-reaction rates are explored in Figure 5. Previously, the relationship between the self-reaction rates of two peroxy radicals and their corresponding cross-reaction rate has been suggested to be two times the geometric mean of the self-reaction rates (Equation 11):[7,11,42]

$$k_{2,R+R',geo} = 2\sqrt{k_{2,R}k_{2,R'}} \tag{11}$$

The relationship between the geometric mean of $k_{2,R}\alpha_{2d,R}$ and $k_{2,R'}\alpha_{2d,R'}$ and the measured $k_{2,R+R'}\alpha_{2d,R+R'}$ for a variety of peroxy radical cross-reactions is given in the left panel of Figure 5.

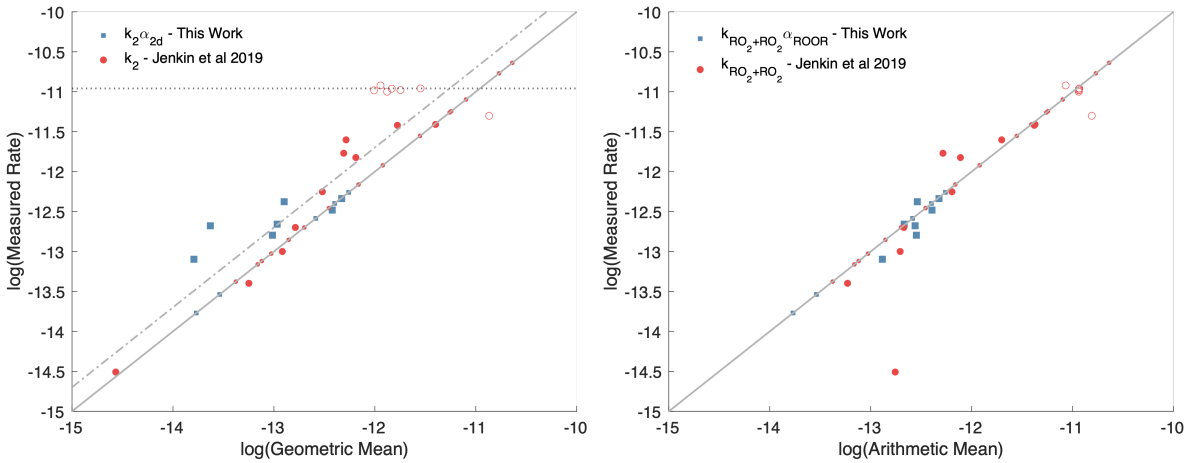

Figure 5: The relationship between the self-reaction and cross-reaction rate constants (k_2) for the peroxy radical systems given in Jenkin et al 2019 (red circles), and the relationship between $k_2\alpha_{2d}$ values for the cross-reactions examined in this study (blue squares). Values for the self-reactions, which fall on the 1:1 line by definition, are plotted as small squares and dots. Open red circles denote data from Jenkin et al that corresponds to a cross-reaction that involves at least one acyl peroxy radical. The left panel shows the relationship between the measured cross reaction rates and the geometric mean of the measured self-reaction rates, while the right panel shows the relationship between the measured cross reaction rates and the arithmetic mean of the measured self-reaction rates. Solid gray lines give the 1:1 line, while the dashed gray line is the 2:1 line. The dotted line in the left panel gives the suggested rate for reactions with acyl peroxy radicals.

These data are compared to the relationship between the geometric means of the measured self-reaction rate constants and the measured cross-reaction rate constants given in Jenkin et al 2019 in the left panel of Figure 5. Cross-reactions that include CH_3O_2 as a reaction partner are slightly different in some cases if the recently measured value of the self-reaction rate constant for CH_3O_2 given in Onel et al is used ($2.0(\pm 0.9)\times 10^{-13}$ cm^3 molecule^{-1} s^{-1}), which is approximately 40% slower than the previously recommended value as given in Jenkin et al.[43] In the right panel of Figure 5, the relationship between the measured cross-reaction rates and the arithmetic mean of the self-reaction rates (Equation 12) is also

plotted with the 1:1 line:

$$k_{2,R+R',ar} = \frac{k_{2,R} + k_{2,R'}}{2} \tag{12}$$

These plots suggest that, while twice the geometric mean has been suggested previously as a method for estimating the cross-reaction rates of peroxy radical systems, the arithmetic mean equally captures this relationship. There is a clear outlier in this trend, the cross-reaction of the tert-butylperoxy radical (t-$C_4H_9O_2$) with the methyl peroxy radical (CH_3O_2). However, the recommended rate coefficient for this reaction is fairly uncertain, and therefore this outlier should not rule out the arithmetic mean as a possible method for estimating the cross reaction.[27,44,45] Indeed, in this study, a simple photochemical box model run of these systems with the cross-reactions given by the arithmetic mean matches the data more closely than a similar run using the geometric mean or twice the geometric mean as the cross-reaction rate. The addition of the factor of two in 11 adds the additional curiosity that in the limiting case where R'=R, $k_{2,R}=2k_{2,R}$. Clearly, further work is needed to develop a robust relationship between the self- and cross-reactions of a variety of peroxy radicals for use in models.

Using the arithmetic mean and measured/estimated rate constants for the self-reactions, we also estimate α_{2d} for each of the cross reactions, and these estimated values are also given in Table 1. Similarly to the $k_2\alpha_{2d}$ values, these values lie in between the α_{2d} values of the corresponding self-reactions.

Conclusion

The kinetics and products of the bimolecular reactions of peroxy radicals in low NO_x environments, including peroxy radical self- and cross-reactions, are crucial to quantify if the ultimate fate and influence of peroxy radical chemistry is to be fully understood. Despite recent increased study of the peroxy radical self-reaction and the formation of the accretion

product via this self-reaction, there is still little information about the formation of this accretion product as a function of structure. In this study, we have added to the current knowledge of these reactions by examining the formation of accretion products in the self- and cross-reaction in primary, secondary, and tertiary peroxy radicals derived from the oxidation of small alkenes by OH. We find that the formation rate of the accretion product depends largely on the substitution of the peroxy radical and decreases with increasing substitution, with no clear dependence on carbon chain length. Further, the formation of the accretion product in the cross-reaction systems yielded formation rates that are well-described by the arithmetic mean of the corresponding self-reactions.

References

(1) Atkinson, R. Gas-Phase Tropospheric Chemistry of Volatile Organic Compounds: 1. Alkanes and Alkenes. *Journal of Physical and Chemical Reference Data* **1997**, *26*, 215–290.

(2) Lightfoot, P. D.; Cox, R. A.; Crowley, J. N.; Destriau, M.; Hayman, G. D.; Jenkin, M. E.; Moortgat, G. K.; Zabel, F. Organic peroxy radicals: Kinetics, spectroscopy and tropospheric chemistry. *Atmospheric Environment. Part A. General Topics* **1992**, *26*, 1805–1961.

(3) Jenkin, M. E.; Clemitshaw, K. C. Ozone and other secondary photochemical pollutants: chemical processes governing their formation in the planetary boundary layer. *Atmospheric Environment* **2000**, *34*, 2499–2527.

(4) Tyndall, G. S.; Cox, R. A.; Granier, C.; Lesclaux, R.; Moortgat, G. K.; Pilling, M. J.; Ravishankara, A. R.; Wallington, T. J. Atmospheric chemistry of small organic peroxy radicals. *Journal of Geophysical Research: Atmospheres* **2001**, *106*, 12157–12182, _eprint: https://onlinelibrary.wiley.com/doi/pdf/10.1029/2000JD900746.

(5) Jenkin, M. E.; Hayman, G. D. Kinetics of reactions of primary, secondary and tertiary -hydroxy peroxyl radicals. *Journal of the Chemical Society, Faraday Transactions* **1995**, *91*, 1911–1922, Publisher: The Royal Society of Chemistry.

(6) Boyd, A. A.; Lesclaux, R.; Jenkin, M. E.; Wallington, T. J. A Spectroscopic, Kinetic, and Product Study of the (CH3)2C(OH)CH2O2 Radical Self Reaction and Reaction with HO2. *The Journal of Physical Chemistry* **1996**, *100*, 6594–6603, Publisher: American Chemical Society.

(7) Orlando, J. J.; Tyndall, G. S. Laboratory studies of organic peroxy radical chemistry: an overview with emphasis on recent issues of atmospheric significance. *Chemical Society Reviews* **2012**, *41*, 6294–6317.

(8) Seinfeld, J. H.; Pandis, S. N. *Atmospheric Chemistry and Physics : From Air Pollution to Climate Change*; Wiley: Hoboken, New Jersey, 2016; Vol. Third edition.

(9) Perring, A. E.; Pusede, S. E.; Cohen, R. C. An Observational Perspective on the Atmospheric Impacts of Alkyl and Multifunctional Nitrates on Ozone and Secondary Organic Aerosol. *Chemical Reviews* **2013**, *113*, 5848–5870, Publisher: American Chemical Society.

(10) Crounse, J. D.; Nielsen, L. B.; Jørgensen, S.; Kjaergaard, H. G.; Wennberg, P. O. Autoxidation of Organic Compounds in the Atmosphere. *The Journal of Physical Chemistry Letters* **2013**, *4*, 3513–3520, Publisher: American Chemical Society.

(11) Jenkin, M. E.; Valorso, R.; Aumont, B.; Rickard, A. R. Estimation of rate coefficients and branching ratios for reactions of organic peroxy radicals for use in automated mechanism construction. *Atmospheric Chemistry and Physics* **2019**, *19*, 7691–7717, Publisher: Copernicus GmbH.

(12) US EPA, O. National Air Quality: Status and Trends of Key Air Pollutants. 2014; `https://www.epa.gov/air-trends`.

(13) Winkler, S. L.; Anderson, J. E.; Garza, L.; Ruona, W. C.; Vogt, R.; Wallington, T. J. Vehicle criteria pollutant (PM, NOx, CO, HCs) emissions: how low should we go? *npj Climate and Atmospheric Science* **2018**, *1*, 1–5, Number: 1 Publisher: Nature Publishing Group.

(14) Wennberg, P. O.; Bates, K. H.; Crounse, J. D.; Dodson, L. G.; McVay, R. C.; Mertens, L. A.; Nguyen, T. B.; Praske, E.; Schwantes, R. H.; Smarte, M. D.; St Clair, J. M.; Teng, A. P.; Zhang, X.; Seinfeld, J. H. Gas-Phase Reactions of Isoprene and Its Major Oxidation Products. *Chemical Reviews* **2018**, *118*, 3337–3390, Publisher: American Chemical Society.

(15) Lee, R.; Gryn'ova, G.; Ingold, K. U.; Coote, M. L. Why are sec-alkylperoxyl bimolecular self-reactions orders of magnitude faster than the analogous reactions of tert-alkylperoxyls? The unanticipated role of CH hydrogen bond donation. *Physical Chemistry Chemical Physics* **2016**, *18*, 23673–23679.

(16) Valiev, R. R.; Hasan, G.; Salo, V.-T.; Kubečka, J.; Kurten, T. Intersystem Crossings Drive Atmospheric Gas-Phase Dimer Formation. *The Journal of Physical Chemistry A* **2019**, *123*, 6596–6604.

(17) Kenseth, C. M.; Huang, Y.; Zhao, R.; Dalleska, N. F.; Hethcox, J. C.; Stoltz, B. M.; Seinfeld, J. H. Synergistic O3 + OH oxidation pathway to extremely low-volatility dimers revealed in -pinene secondary organic aerosol. *Proceedings of the National Academy of Sciences* **2018**, *115*, 8301–8306, Publisher: Proceedings of the National Academy of Sciences.

(18) Peräkylä, O.; Berndt, T.; Franzon, L.; Hasan, G.; Meder, M.; Valiev, R. R.; Daub, C. D.; Varelas, J. G.; Geiger, F. M.; Thomson, R. J.; Rissanen, M.; Kurtén, T.; Ehn, M. Large Gas-Phase Source of Esters and Other Accretion Products in the Atmosphere.

Journal of the American Chemical Society **2023**, *145*, 7780–7790, Publisher: American Chemical Society.

(19) Berndt, T.; Mentler, B.; Scholz, W.; Fischer, L.; Herrmann, H.; Kulmala, M.; Hansel, A. Accretion Product Formation from Ozonolysis and OH Radical Reaction of -Pinene: Mechanistic Insight and the Influence of Isoprene and Ethylene. *Environmental Science & Technology* **2018**, *52*, 11069–11077.

(20) Molteni, U. et al. Formation of Highly Oxygenated Organic Molecules from -Pinene Ozonolysis: Chemical Characteristics, Mechanism, and Kinetic Model Development. *ACS Earth and Space Chemistry* **2019**, *3*, 873–883.

(21) Kwan, A. J.; Chan, A. W. H.; Ng, N. L.; Kjaergaard, H. G.; Seinfeld, J. H.; Wennberg, P. O. Peroxy radical chemistry and OH radical production during the NO_3-initiated oxidation of isoprene. *Atmospheric Chemistry and Physics* **2012**, *12*, 7499–7515, Publisher: Copernicus GmbH.

(22) Berndt, T.; Richters, S.; Kaethner, R.; Voigtländer, J.; Stratmann, F.; Sipilä, M.; Kulmala, M.; Herrmann, H. Gas-Phase Ozonolysis of Cycloalkenes: Formation of Highly Oxidized RO2 Radicals and Their Reactions with NO, NO2, SO2, and Other RO2 Radicals. *The Journal of Physical Chemistry A* **2015**, *119*, 10336–10348, Publisher: American Chemical Society.

(23) Lee, B. H.; Lopez-Hilfiker, F. D.; D'Ambro, E. L.; Zhou, P.; Boy, M.; Petäjä, T.; Hao, L.; Virtanen, A.; Thornton, J. A. Semi-volatile and highly oxygenated gaseous and particulate organic compounds observed above a boreal forest canopy. *Atmospheric Chemistry and Physics* **2018**, *18*, 11547–11562.

(24) Murphy, S. E.; Crounse, J. D.; Møller, K. H.; Rezgui, S. P.; Hafeman, N. J.; Park, J.; Kjaergaard, H. G.; Stoltz, B. M.; Wennberg, P. O. Accretion product formation in

the self-reaction of ethene-derived hydroxy peroxy radicals. *Environmental Science: Atmospheres* **2023**, Publisher: RSC.

(25) Yue, H.; Zhang, C.; Lin, X.; Wen, Z.; Zhang, W.; Mostafa, S.; Luo, P.-L.; Zhang, Z.; Hemberger, P.; Fittschen, C.; Tang, X. Dimeric Product of Peroxy Radical Self-Reaction Probed with VUV Photoionization Mass Spectrometry and Theoretical Calculations: The Case of C2H5OOC2H5. *International Journal of Molecular Sciences* **2023**, *24*, 3731.

(26) Liu, L.; Zhang, C.; Xia, Y.; Zhang, W.; Wang, Z.; Tang, X. Dimeric product formation in the self-reaction of small peroxy radicals using synchrotron radiation vacuum ultraviolet photoionization mass spectrometry. *Chemosphere* **2024**, *363*, 142846.

(27) Atkinson, R.; Baulch, D. L.; Cox, R. A.; Crowley, J. N.; Hampson, R. F.; Hynes, R. G.; Jenkin, M. E.; Rossi, M. J.; Troe, J.; Subcommittee, I. Evaluated kinetic and photochemical data for atmospheric chemistry: Volume II – gas phase reactions of organic species. *Atmospheric Chemistry and Physics* **2006**, *6*, 3625–4055, Publisher: Copernicus GmbH.

(28) Vasquez, K. T.; Allen, H. M.; Crounse, J. D.; Praske, E.; Xu, L.; Noelscher, A. C.; Wennberg, P. O. Low-pressure gas chromatography with chemical ionization mass spectrometry for quantification of multifunctional organic compounds in the atmosphere. *Atmospheric Measurement Techniques* **2018**, *11*, 6815–6832.

(29) Paulot, F.; Crounse, J. D.; Kjaergaard, H. G.; Kroll, J. H.; Seinfeld, J. H.; Wennberg, P. O. Isoprene photooxidation: new insights into the production of acids and organic nitrates. *Atmospheric Chemistry and Physics* **2009**, *9*, 1479–1501, Publisher: Copernicus GmbH.

(30) St. Clair, J. M.; Spencer, K. M.; Beaver, M. R.; Crounse, J. D.; Paulot, F.; Wennberg, P. O. Quantification of hydroxyacetone and glycolaldehyde using chemical

ionization mass spectrometry. *Atmospheric Chemistry and Physics* **2014**, *14*, 4251–4262, Publisher: Copernicus GmbH.

(31) Crounse, J. D.; Paulot, F.; Kjaergaard, H. G.; Wennberg, P. O. Peroxy radical isomerization in the oxidation of isoprene. *Physical Chemistry Chemical Physics* **2011**, *13*, 13607–13613, Publisher: The Royal Society of Chemistry.

(32) Hyttinen, N.; Otkjær, R. V.; Iyer, S.; Kjaergaard, H. G.; Rissanen, M. P.; Wennberg, P. O.; Kurtén, T. Computational Comparison of Different Reagent Ions in the Chemical Ionization of Oxidized Multifunctional Compounds. *The Journal of Physical Chemistry A* **2018**, *122*, 269–279, Publisher: American Chemical Society.

(33) Crounse, J. D.; McKinney, K. A.; Kwan, A. J.; Wennberg, P. O. Measurement of Gas-Phase Hydroperoxides by Chemical Ionization Mass Spectrometry. *Analytical Chemistry* **2006**, *78*, 6726–6732.

(34) Su, T.; Chesnavich, W. J. Parametrization of the ion–polar molecule collision rate constant by trajectory calculations. *The Journal of Chemical Physics* **1982**, *76*, 5183–5185.

(35) Garden, A. L.; Paulot, F.; Crounse, J. D.; Maxwell-Cameron, I. J.; Wennberg, P. O.; Kjaergaard, H. G. Calculation of conformationally weighted dipole moments useful in ion–molecule collision rate estimates. *Chemical Physics Letters* **2009**, *474*, 45–50.

(36) O'Haver, T. Interactive Peak Fitter. 2017; `https://terpconnect.umd.edu/~toh/spectrum/InteractivePeakFitter.htm`.

(37) Sharpe, S. W.; Sams, R. L.; Johnson, T. J. The PNNL Quantitative IR Database for Infrared Remote Sensing and Hyperspectral Imaging. Proceedings of the 31st Applied Image Pattern Recognition Workshop on From Color to Hyperspectral: Advancements in Spectral Imagery Exploitation. USA, 2002; pp 45–48.

(38) Teng, A. P.; Crounse, J. D.; Lee, L.; St. Clair, J. M.; Cohen, R. C.; Wennberg, P. O. Hydroxy nitrate production in the OH-initiated oxidation of alkenes. *Atmospheric Chemistry and Physics* **2015**, *15*, 4297–4316, Publisher: Copernicus GmbH.

(39) Xu, L.; Møller, K. H.; Crounse, J. D.; Otkjær, R. V.; Kjaergaard, H. G.; Wennberg, P. O. Unimolecular Reactions of Peroxy Radicals Formed in the Oxidation of {α}-Pinene and β-Pinene by Hydroxyl Radicals. *The Journal of Physical Chemistry A* **2019**, *123*, 1661–1674.

(40) Chakir, A.; P. Ganne, J.; Roth, E.; Brion, J.; Daumont, D. Study of (CH 3) 2 C(OH)CH 2 O 2 using modulated photolysis: ultra-violet spectrum and self-reaction kinetics. *Physical Chemistry Chemical Physics* **2004**, *6*, 3389–3395, Publisher: Royal Society of Chemistry.

(41) Boyd, A. A.; Villenave, E.; Lesclaux, R. Self- and cross-reactions of -hydroxyperoxy radicals of relevance to tropospheric monoterpene oxidation: structure–activity relationships for rate coefficients. *Atmospheric Environment* **2003**, *37*, 2751–2760.

(42) Madronich, S.; Calvert, J. G. Permutation reactions of organic peroxy radicals in the troposphere. *Journal of Geophysical Research: Atmospheres* **1990**, *95*, 5697–5715, _eprint: https://onlinelibrary.wiley.com/doi/pdf/10.1029/JD095iD05p05697.

(43) Onel, L.; Brennan, A.; Østerstrom, F. F.; Cooke, E.; Whalley, L.; Seakins, P. W.; Heard, D. E. Kinetics and Product Branching Ratio Study of the CH3O2 Self-Reaction in the Highly Instrumented Reactor for Atmospheric Chemistry. *The Journal of Physical Chemistry A* **2022**, *126*, 7639–7649, Publisher: American Chemical Society.

(44) Parkes, D. 15th International Symposium on Combustion (The Combustion Institute, Pittsburgh, 1975). 1975; p p. 795.

(45) Osborne, D. A.; Waddington, D. J. Reactions of oxygenated radicals in the gas phase. Part 14. Reactions of t-butylperoxyl radicals. **1984**, 1861–1867.